

Coexistence of quasi-two dimensional electron and hole gas in a single tier $\text{Ca}_{0.5}\text{TaO}_3/\text{SrTiO}_3$ oxide heterostructure

Cite as: APL Mater. 7, 071108 (2019); <https://doi.org/10.1063/1.5109631>

Submitted: 10 May 2019 . Accepted: 19 June 2019 . Published Online: 17 July 2019

J. J. Pulikkotil



View Online



Export Citation



CrossMark

ARTICLES YOU MAY BE INTERESTED IN

[Self-assembly and properties of domain walls in \$\text{BiFeO}_3\$ layers grown via molecular-beam epitaxy](#)

APL Materials 7, 071101 (2019); <https://doi.org/10.1063/1.5103244>

[Large tetragonality and room temperature ferroelectricity in compressively strained \$\text{CaTiO}_3\$ thin films](#)

APL Materials 7, 051104 (2019); <https://doi.org/10.1063/1.5090798>

[Revealing surface-state transport in ultrathin topological crystalline insulator \$\text{SnTe}\$ films](#)

APL Materials 7, 051106 (2019); <https://doi.org/10.1063/1.5096279>

additive manufacturing epitaxial crystal growth cerium oxide polishing powder silver nanoparticles sputtering targets

THE ADVANCED MATERIALS MANUFACTURER®

deposition slugs OLED Lighting spintronics solar energy

osmium nanoribbons thin films chalcogenides AuNPs

GDC li-ion battery electrolytes 99.999% ruthenium spheres

endohedral fullerenes copper nanoparticles diamond micropowder

CIGS MBE grade materials palladium catalysts flexible electronics

beta-barium borate borosilicate glass dysprosium pellets YBCO

pyrolytic graphite 3d graphene foam indium tin oxide mesoporous silica

raman substrates sapphire windows tungsten carbide InGaAs

barium fluoride carbon nanotubes lithium niobate scandium powder

Now Invent.™

The Next Generation of Material Science Catalogs

III-IV semiconductors CVD precursors europium phosphors

InAs wafers laser crystals ultra high purity materials MOFs

rare earth metals photovoltaics refractory metals MOCVD

superconductors transparent ceramics ultra high purity silicon

*American Elements opens up a world of possibilities so you can **Now Invent!***

Over 15,000 certified high purity laboratory chemicals, metals, & advanced materials and a state-of-the-art Research Center. Printable GHS-compliant Safety Data Sheets. Thousands of new products. And much more. All on a secure multi-language "Mobile Responsive" platform.

perovskite crystals yttrium iron garnet alternative energy h-BN

gold nanocubes graphene oxide macromolecules photonics

rhodium sponge fiber optics beamsplitters infrared dyes zeolites

fused quartz metallocenes platinum ink buckyballs Ti-6Al-4V

www.americanelements.com



Coexistence of quasi-two dimensional electron and hole gas in a single tier $\text{Ca}_{0.5}\text{TaO}_3/\text{SrTiO}_3$ oxide heterostructure

Cite as: APL Mater. 7, 071108 (2019); doi: 10.1063/1.5109631

Submitted: 10 May 2019 • Accepted: 19 June 2019 •

Published Online: 17 July 2019



View Online



Export Citation



CrossMark

J. J. Pulikkotil

AFFILIATIONS

CSIR-National Physical Laboratory, Dr. K. S. Krishnan Marg, New Delhi 110012, India

ABSTRACT

Quasi-two-dimensional electron gas has been realized at the polar-nonpolar interface of several insulating oxide heterostructures. However, its hole counterpart remains elusive. In an attempt to find a novel system that exhibits quasi-two-dimensional hole gas (q-2DHG) at the heterointerface, we adopt to materials search, first based on phenomenology followed by a comprehensive set of calculations based on first-principles density functional theory. Our studies show the epitaxial growth of cubic $\text{Ca}_{0.5}\text{TaO}_3$ on TiO_2 terminated substrate display (q-2DHG). The hole gas emanates from the O $2p$ orbitals of the TiO_2 layers of the substrate. On the other hand, an electron gas is formed at the (001) TaO_2 top surface, thereby representing the heterostructure as a coupled quantum well system. The partial filling of the Ta $5d_{2g}$ conduction band indicates electron reconstruction, in agreement with the polar catastrophe model. Besides, a critical thickness of three monolayers is deduced from the calculations for the formation of q-2DHG in the $\text{Ca}_{0.5}\text{TaO}_3/\text{SrTiO}_3$ heterostructure, which is consistent with the model prediction based on the modern theory of polarization. With both cubic systems, $\text{Ca}_{0.5}\text{TaO}_3$ and SrTiO_3 , having a similar underlying symmetry and minimal lattice mismatch, epitaxial growth with an abrupt interface can be well anticipated. Such a single-tier oxide heterostructure composed of separated confined hole-electron subsystems is expected to provide a platform to unravel exciting physics and also for functional devices related to oxide electronics.

© 2019 Author(s). All article content, except where otherwise noted, is licensed under a Creative Commons Attribution (CC BY) license (<http://creativecommons.org/licenses/by/4.0/>). <https://doi.org/10.1063/1.5109631>

The origin of quasi-two-dimensional electron gas at the interface of polar and nonpolar insulating oxides has been attributed to several mechanisms, such as oxygen defects, intersite cation disorder, atomic reconstruction, and electronic reconstruction.¹⁻⁹ Of these, the most fascinating is the electronic reconstruction at the heterointerface due to the polar catastrophe model. In this model, an abrupt heterointerface between polar and nonpolar insulating oxides manifests a polarity discontinuity, thereby resulting in an electric potential which diverges with the increasing thickness of the overlayer polar film. As a result, the heterointerface becomes electronically unstable. To nullify the built-in potential, the polar catastrophe model proposes an electronic reconstruction at the heterointerface. For instance, in case of $\text{LaAlO}_3/\text{SrTiO}_3$, an electronic reconstruction occurs in the vicinity of the TiO_2 heterointerface, with an amalgam of Ti^{4+} and Ti^{3+} states. The n -type carriers generated are, however, confined to a narrow region, thereby resulting in a quasi-two-dimensional electron gas (q-2DEG).

While several such oxide heterostructures exhibiting q-2DEG have been tailored successfully,^{10,11} its counterpart, i.e., the quasi-two-dimensional hole gas (q-2DHG), has not been realized in single-tier oxide heterostructures. Rather, such p -type heterointerfaces have been found insulating.¹²⁻¹⁴ However, a q-2DHG has been experimentally discovered in a two-tier $\text{SrTiO}_3/\text{LaAlO}_3/\text{SrTiO}_3$ heterostructure.¹⁵ Two confined conducting channels with $(\text{LaO})^+/\text{(TiO}_2)^0$ heterointerface exhibiting n -type conductivity and $(\text{AlO}_2)^-/\text{(SrO)}^0$ interface showing a p -type conductivity were observed in this system.¹⁵

Realizing that n -type heterointerfaces are more common than the p -type counterparts, we attempt to envisage the latter in a new heterostructure using density functional theory calculations. To look for an appropriate oxide that can be epitaxially grown on SrTiO_3 , we adhere to the fundamental assumptions of the polar catastrophe model, i.e., the overlayer oxide must be polar and must also have minimal lattice mismatch with the substrate. In this view, we

carried out a materials objective search using the Crystallography Open Database^{16,17} and found $\text{Ca}_{0.5}\text{TaO}_3$ ¹⁸ to be a good material to realize q -2DHG. The advantage of $\text{Ca}_{0.5}\text{TaO}_3$ is that it has a underlying cubic symmetry (space group: Pm-3m) with lattice constant $a = 3.875 \text{ \AA}$. In comparison to SrTiO_3 ($a = 3.905 \text{ \AA}$), the lattice mismatch of $\text{Ca}_{0.5}\text{TaO}_3/\text{SrTiO}_3$ is then estimated to be $\approx 0.7\%$. Besides, the Ca vacancies offer an opposite stacking of polar layers in comparison to LaAlO_3 . In $\text{LaAlO}_3/\text{SrTiO}_3$, the positively charged $(\text{LaO})^+$ and the charge neutral $(\text{TiO}_2)^0$ layers constitute the heterointerface. On the other hand, in $\text{Ca}_{0.5}\text{TaO}_3/\text{SrTiO}_3$, the heterointerface is realized as $\dots/(\text{TiO}_2)^0/(\text{Ca}_{0.5}\text{O})^-/(\text{TaO}_2)^+\dots$, where a negatively charged $(\text{Ca}_{0.5}\text{O})^-$ comes in contact with the $(\text{TiO}_2)^0$ layer of the substrate. The negatively charged $(\text{Ca}_{0.5}\text{O})^-/(\text{TiO}_2)^0$ layer resembles much like the $(\text{AlO}_2)^-/(\text{SrO})^0$, the latter in which a p -type conductivity has been reported.¹⁵ The $\text{Ca}_{0.5}\text{TaO}_3/\text{SrTiO}_3$ interface is shown schematically in Fig. 1.

Thus, finding that the lattice mismatch is minimal and that a p -type interface can be formed in $\text{Ca}_{0.5}\text{TaO}_3/\text{SrTiO}_3$, we performed a comprehensive set of calculations based on first-principles density functional theory. Consistent with the predictions of the polar catastrophe theory, we found an accumulation of p -type charge carriers at the heterointerface of $\text{Ca}_{0.5}\text{TaO}_3/\text{SrTiO}_3$. In fact, the onset of conductivity is seen above certain critical thickness of the $\text{Ca}_{0.5}\text{TaO}_3$ overlayers. The emergence of hole conductivity is charge compensated by an electronic reconstruction of the Ta ions on the TaO_2 surface layer. Therefore, $\text{Ca}_{0.5}\text{TaO}_3/\text{SrTiO}_3$ represents a p -type oxide heterostructure, the experimental synthesis and characterization of which can lead to a leap in oxide electronics applications. Furthermore, the spatial separation of the nonequilibrium charge carriers can cause nanometer scale variations in the electrostatic potential, thereby having significant impact on the generation, recombination, and transport of charge carriers.

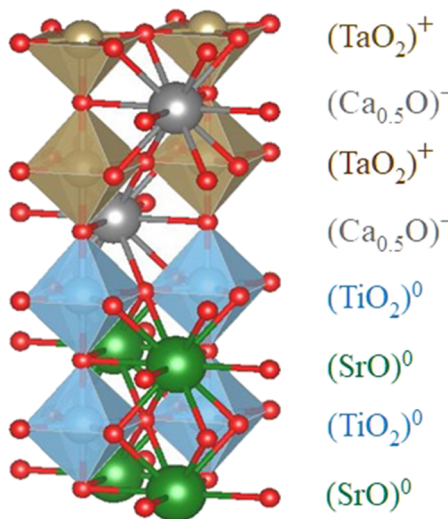


FIG. 1. Schematic representation of the heterointerface geometry of the $\text{Ca}_{0.5}\text{TaO}_3/\text{SrTiO}_3$ heterostructure. The various atoms are Ca (gray), Ti (blue), O (red), and Sr (green), and Ta (brown). The polarity of the layers is also shown with TiO_2 and SrO being charge neutral and $(\text{Ca}_{0.5}\text{O})^-$ and $(\text{TaO}_2)^+$ being negatively and positively charged, respectively.

All electron full potential linearized augmented plane-wave (FP-LAPW) method as implemented in the Wien2k code¹⁹ was employed to study the structural and electronic structure properties of $\text{Ca}_{0.5}\text{TaO}_3/\text{SrTiO}_3$ heterostructures. These were modeled using supercells of dimension $\sqrt{2}a \times \sqrt{2}a \times 2an$, where a ($=3.905 \text{ \AA}$) was taken to be that of cubic SrTiO_3 and n , the number of monolayers (MLs). A monolayer (ML) is defined as a $\text{Ca}_{0.5}\text{O}/\text{TaO}_2$ unit in the $\text{Ca}_{0.5}\text{TaO}_3$ overlayer film and a SrO/TiO_2 unit in the SrTiO_3 substrate along the crystallographic $[001]$ direction. The TiO_2 terminated SrTiO_3 substrate in our model calculations has five MLs, and the thickness of the $\text{Ca}_{0.5}\text{TaO}_3$ was varied from 1 to 4 ML. The LAPW sphere radii for Sr/Ca, Ti/Ta, and O were chosen as 2.2, 1.9, and 1.6 a.u., respectively. The internal coordinates of all ions constituting the heterostructure were relaxed. The ground state properties were obtained using well-converged basis sets using the Wien2k parameters: $R_{\text{MT}}K_{\text{max}} = 7$, $G_{\text{max}} = 24 \text{ a.u.}^{-1}$, and $l_{\text{max}} = 7$.¹⁹ The exchange correlation potential to the crystal Hamiltonian was considered in Generalized Gradient Approximation (GGA) as prescribed by Perdew, Burke, and Ernzerhof (PBE).²⁰ The Brillouin Zone (BZ) integration was carried out using the modified tetrahedron method with a mesh size of $12 \times 12 \times 2$, yielding 98k-points in its irreducible wedge.

Prelude to understand the properties of the $\text{Ca}_{0.5}\text{TaO}_3/\text{SrTiO}_3$ heterostructures, we first determined the structural and electronic structure properties of cubic $\text{Ca}_{0.5}\text{TaO}_3$. The material was modeled using a cubic unit cell with the underlying Fm-3m (space group 225) symmetry. Ca ions were positioned at the $4a$ $(0, 0, 0)$ Wyck-off position, Ta ions at $8c$ $(\frac{1}{4}, \frac{1}{4}, \frac{1}{4})$, and O ions at $(\frac{1}{4}, 0, \frac{1}{4})$ position of the face centered cubic unit cell. Total energy enroute to determine the equilibrium lattice constant determined the value $a_0 = 3.968 \text{ \AA}$ for $\text{Ca}_{0.5}\text{TaO}_3$. In comparison to the experiments, the theoretically determined lattice constant was $\approx 2.4\%$ overestimated, which can be considered legitimate within the scope of GGA-PBE formalism of treating exchange-correlation effects. The band structure and density of states (DOS) spectra of $\text{Ca}_{0.5}\text{TaO}_3$ are shown in Fig. 2(a). Generic to all cubic oxide perovskites, the upper valence bands are dominated by the O $2p$ bands, while the conduction bands were composed of the Ta $5d$ -bands. An insulating ground state with an electronic gap (E_g) of 2.15 eV was determined using GGA-PBE against the experimental value of 4.0 eV.²¹

The overestimation of lattice constant and the underestimation of the electronic gap is quite inherent in GGA-PBE. Therefore, to compare the theoretically obtained values with experiments, we calculated the same physical quantities for cubic SrTiO_3 under a similar set of approximations and computational parameters. We found a_0 for SrTiO_3 to be $\approx 3.938 \text{ \AA}$, which is barely 0.9% overestimated compared to the experimental value of 3.905 \AA . The electronic structure calculated at the equilibrium lattice constant for SrTiO_3 is shown in Fig. 2(b). Note that for a direct comparison of the electronic structure of SrTiO_3 with that of $\text{Ca}_{0.5}\text{TaO}_3$, we calculated the band structure and DOS spectra for SrTiO_3 using a 2 f.u. unit cell with the underlying Fm-3m cubic symmetry. The E_g for SrTiO_3 was estimated to be $\approx 1.87 \text{ eV}$. From these sets of calculations, it becomes evident that GGA-PBE consistently underestimates the E_g of band insulators, such as SrTiO_3 and $\text{Ca}_{0.5}\text{TaO}_3$, by $\approx 55\%$ – 60% .

Although discrepancies exist between the theoretical and experimental values, the calculations provide qualitatively good

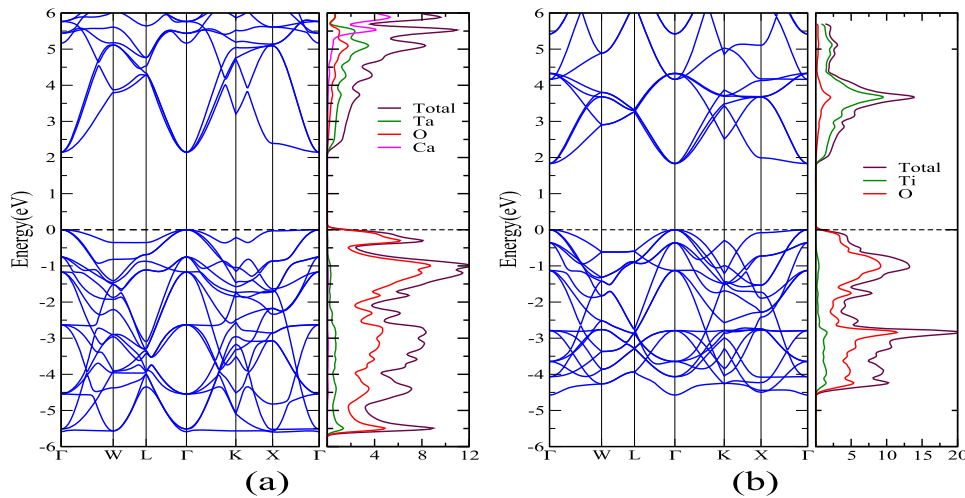


FIG. 2. The GGA computed band structure and DOS of (a) $\text{Ca}_{0.5}\text{TaO}_3$ and (b) SrTiO_3 calculated using the Fm-3m underlying cubic symmetry for a direct comparison. The vertical broken line along energy zero represents the reference Fermi energy. In the DOS spectra, the atom resolved partial DOS are also shown.

results. For instance, the experimental lattice mismatch between $\text{Ca}_{0.5}\text{TaO}_3$ and SrTiO_3 amounts to 0.7%, while the theoretical values amount to 0.8%. Thus, based on the underlying cubic symmetry and minimal lattice mismatch between $\text{Ca}_{0.5}\text{TaO}_3$ and SrTiO_3 , we predict that the epitaxial growth of $\text{Ca}_{0.5}\text{TaO}_3$ films is possible on the SrTiO_3 substrate. Also, consistent with the experiments, the GGA-PBE calculations predict $E_g(\text{Ca}_{0.5}\text{TaO}_3) > E_g(\text{SrTiO}_3)$. This infers that the electronic gap of SrTiO_3 would completely lie within the gap of $\text{Ca}_{0.5}\text{TaO}_3$. As a result, the charge carriers if generated at the heterointerface can be anticipated to reside in the SrTiO_3 side of the heterointerface, similar to $\text{LaAlO}_3/\text{SrTiO}_3$ oxide heterostructures.

Having realized that $\text{Ca}_{0.5}\text{TaO}_3$ can be modeled as alternating negative $(\text{Ca}_{0.5}\text{O})^-$ and positive $(\text{TaO}_2)^+$ layers on TiO_2 terminated

SrTiO_3 substrate and epitaxial growth with an abrupt interface is possible, polar catastrophe theory anticipates conductivity at the heterointerface. Nevertheless, one of the important predictions of the model is that there exists an overlayer film thickness threshold for heterointerface conductivity to emerge.²⁶ Hence, we have modeled heterostructures with varying thickness (1–4 ML) of $\text{Ca}_{0.5}\text{TaO}_3$ on TiO_2 terminated SrTiO_3 . Also, since the interplay of electrostatic effects and local lattice distortions is crucial in determining the electronic structure properties of oxide heterostructures, we first present the structural relaxation effects in the 1–4 ML $\text{Ca}_{0.5}\text{TaO}_3/\text{SrTiO}_3$ oxide heterostructures.

Figure 3 graphically summarizes the results of the structural relaxation effects in $\text{Ca}_{0.5}\text{TaO}_3/\text{SrTiO}_3$ heterostructures for the overlayer film thickness ranging from 1 to 4 ML. By large, the effect

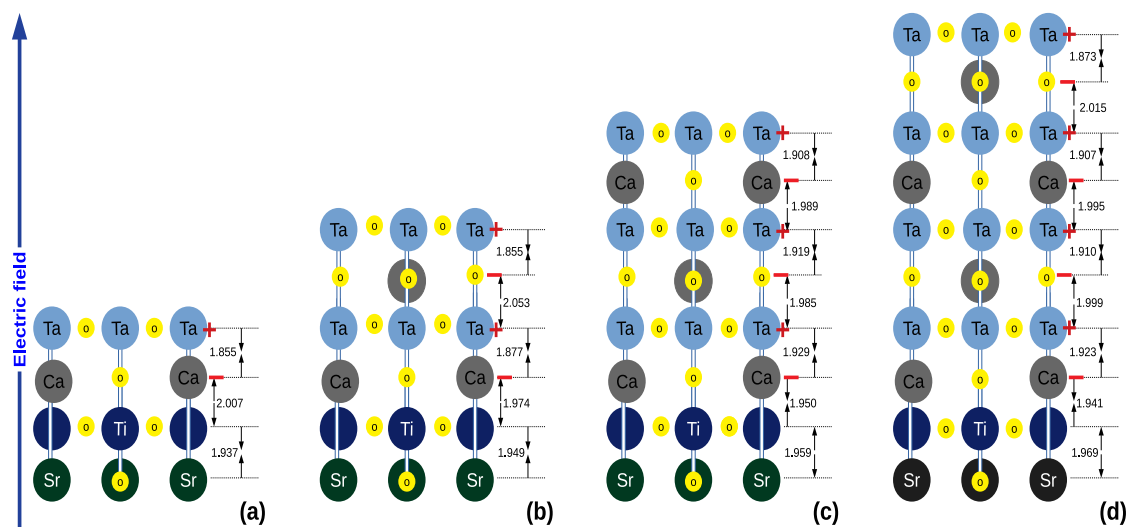


FIG. 3. The results of the GGA structural optimization shown in terms of interlayer distance (in Å) between the charged $(\text{Ca}_{0.5}\text{O})^-$ and $(\text{TaO}_2)^+$ layers of $\text{Ca}_{0.5}\text{TaO}_3/\text{SrTiO}_3$ heterostructures for (a) 1 ML, (b) 2 ML, (c) 3 ML, and (d) 4 ML $\text{Ca}_{0.5}\text{TaO}_3$ overlayer thickness. The directions of the arrows between the layers indicate the elongation (arrows pointing outwards) and compression (arrows pointing inwards) of the planes with respect to the interplanar distance of SrTiO_3 (1.952 Å). The green, blue, and yellow geometries represent Sr, Ti, and O ions, respectively, while the turquoise and gray represent the Ta and Ca ions, respectively.

of structural relaxation is mostly seen in the $\text{Ca}_{0.5}\text{TaO}_3$ overlayers. In the substrate, the distortion is largely contained in the TiO_6 octahedra which is in the immediate vicinity of the heterointerface. The interplanar distance between the TiO_2 and SrO layers of the substrate in its interior corresponds to that of the bulk value, i.e., $d_{\text{STO}} = 1.952 \text{ \AA}$. However, the TiO_2 - SrO interplanar distance which constitutes the heterointerface ML shows a systematic change in their separation with increasing overlayer thickness. While for 1 ML $\text{Ca}_{0.5}\text{TaO}_3$ its separation decreases by -0.8% from that of d_{STO} , it steadily increases to $+0.9\%$ for 4 ML $\text{Ca}_{0.5}\text{TaO}_3$. Thus, we find that increasing the $\text{Ca}_{0.5}\text{TaO}_3$ film thickness above 2 ML leads to an inversion of the TiO_6 distortion pattern at the heterointerface. Such distortions, which result in the elongation of the TiO_6 octahedra at the heterointerface, have been argued to facilitate conductivity.^{22,23}

Besides, we find that planes along the $[001]$ crystallographic direction are alternately compressed and elongated. For the 4 ML $\text{Ca}_{0.5}\text{TaO}_3/\text{SrTiO}_3$ heterostructure, as large as 5% change in the interplanar distances has been estimated for the surface and subsurface TaO_2 layer with the adjacent $\text{Ca}_{0.5}\text{O}$ layer. The in-plane and out-of-plane Ta-O bond distances range between 1.88 \AA and 2.01 \AA . On the contrary, the Ti-O distortion in the substrate is found very minimal within a value of $\approx 0.01 \text{ \AA}$ or smaller. Furthermore, the deviation of the Ti-O-Ti bond angle from 180° is found to be $< 1.5^\circ$, whereas the Ta-O-Ta bond angle in the surface TaO_2 layer deviates by $\approx 3^\circ$. Thus, the structural relaxation of the heterostructure shows significant distortion in the TaO_6 octahedra, which is then expected to lift the degeneracy of the Ta $5d_{2g}$ orbitals.

The elongation and compression of alternate layers in the $\text{Ca}_{0.5}\text{TaO}_3/\text{SrTiO}_3$ heterostructures, irrespective of the ML thickness, partly validates the polar catastrophe model. This can be interpreted as a response to the built-in electric field due to the polar-nonpolar interface. This electric field polarization vector is directed perpendicular to the surface. Along this field direction, the internal field between the $(\text{Ca}_{0.5}\text{O})^- \rightarrow (\text{TaO}_2)^+$ layers is then oppositely directed to the polarization, while that of $(\text{TaO}_2)^+ \rightarrow (\text{Ca}_{0.5}\text{O})^-$ is parallel. As a result, the interplanar distance between the $(\text{Ca}_{0.5}\text{O})^--(\text{TaO}_2)^+$ layers along the crystallographic c -axis is elongated

and the $(\text{TaO}_2)^+--(\text{Ca}_{0.5}\text{O})^-$ is compressed. Such effects have also been observed in $\text{LaAlO}_3/\text{SrTiO}_3$ heterostructures.^{24,25} The interplanar distances shown in Fig. 3 represent averaged quantities.

We also observe a trend in the interlayer separation between the $\langle (\text{Ca}_{0.5}\text{O})^- - (\text{TaO}_2)^+ \rangle$ layers and $\langle (\text{TaO}_2)^+ - (\text{Ca}_{0.5}\text{O})^- \rangle$ layers along the growth direction, i.e., the crystallographic c -axis. For instance, in the 4 ML heterostructure, the $\langle (\text{Ca}_{0.5}\text{O})^- - (\text{TaO}_2)^+ \rangle$ separation decreases steadily from 1.923 \AA (near to the heterointerface) to 1.873 \AA (the surface layer), i.e., a decrease by -2.7% . On the other hand, the $\langle (\text{TaO}_2)^+ - (\text{Ca}_{0.5}\text{O})^- \rangle$ layer separation increases by 0.8% i.e., from 1.999 \AA to 2.015 \AA (the subsurface layer). Similarly, for the 2 ML heterostructure, the relative decrease in the two $\langle (\text{Ca}_{0.5}\text{O})^- - (\text{TaO}_2)^+ \rangle$ layer separations is estimated to be -1.1% . These observations are consistent with the assumptions of the polar catastrophe model that the layers of such polar-nonpolar oxide heterostructures can be approximated as parallel plate capacitors. The relative increase (decrease) in the interplanar distances between the charged layers along the c -axis with increasing film thickness is clearly a manifestation of a proportional increase in the built-in potential with increasing ML thickness. Thus, we find that density functional based calculations capture the essential model characteristics pertained to the polar catastrophe theory. The interplay of electrostatic effects and local lattice distortions is evident from the calculations.

The electronic structures of the $\text{Ca}_{0.5}\text{TaO}_3/\text{SrTiO}_3$ heterostructures for 1–4 ML overlayers are studied in terms of DOS, charge, and orbital populations. In Figs. 4(a)–4(d), we show the thickness dependent evolution of the electronic structure of the $\text{Ca}_{0.5}\text{TaO}_3/\text{SrTiO}_3$ heterostructure. The 1 ML $\text{Ca}_{0.5}\text{TaO}_3/\text{SrTiO}_3$ heterostructure is insulating with $E_g \approx 0.72 \text{ eV}$, and the 2 ML heterostructure is found barely insulating. For $\text{Ca}_{0.5}\text{TaO}_3$ overlayers ≥ 3 ML, there appears finite density of states at the Fermi energy, rendering a metallic ground state. The valence band of all four heterostructure systems is composed of the O $2p$ bands, while the conduction band is composed of the transition metal d states. However, the $3d$ states of the Ti ions of the substrate were found to be 0.5 eV above the surface Ta $5d$ bands.

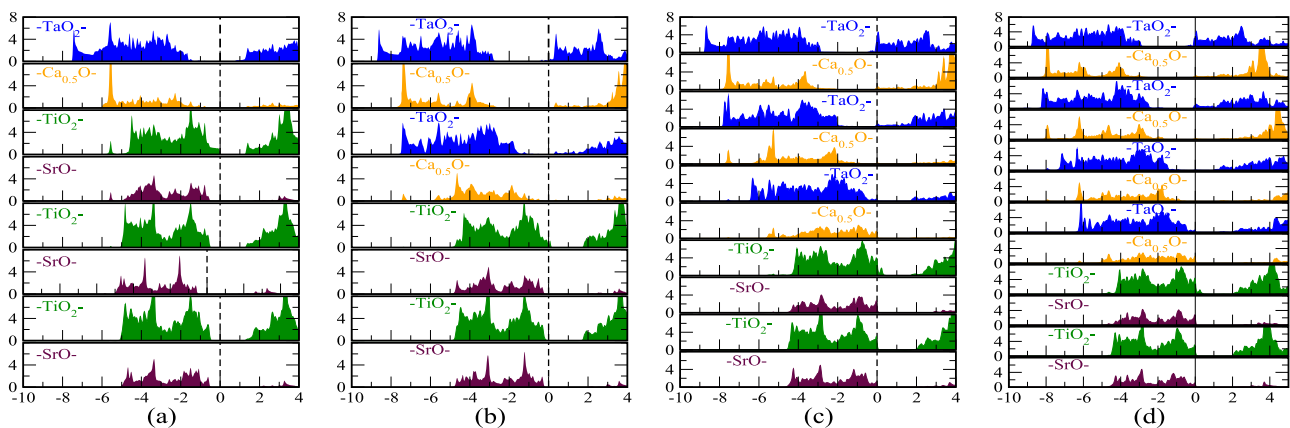


FIG. 4. The layer wise projected density of states (in St./eV , along vertical axis) of (a) 1 ML, (b) 2 ML, (c) 3 ML, and (d) 4 ML $\text{Ca}_{0.5}\text{TaO}_3/\text{SrTiO}_3$ heterostructures. The horizontal axis represents the energy variation, with the broken line along energy zero representing the reference Fermi energy.

Evidently, a substantial band bending is manifested in the electronic structure by a layer wise change in the position of the valence band maximum (VBM) and conduction band minimum (CBM). In fact, this variation reflects the electrostatic potential which rigidly shift the bands with respect to the Fermi energy. Together with the changes observed in the interlayer separation and the band bending effects, a strong correlation of the electrostatic effects with that of the electronic structure becomes evident as a function of increasing film thickness. In particular, it may be followed from the above discussion that the TaO₂ surface layer is significantly compressed along the *c*-axial direction of the heterostructure. This enhances the hybridization between the Ta 5*d* and O 2*p* orbitals of adjacent layers, thereby increasing the covalency associated with the surface chemical bonds.

We now calculate the critical thickness (t_C) of the Ca_{0.5}TaO₃ films which will introduce charge carriers at the heterointerface. The potential divergence resulting in band bending equates with the E_g of Ca_{0.5}TaO₃, which for bulk is ≈ 4.0 eV.²¹ Besides, the potential difference between the surface and interface can be approximated as $ea_0 E_{pol} t_C$, with the polar field $E_{pol} = 2\pi e/\epsilon a_0^2$, a_0 being the lattice constant and ϵ being the dielectric constant of Ca_{0.5}TaO₃. Thus, given $E_g = 4.0$ eV and assuming $\epsilon \approx 25$, t_C is estimated to be ≈ 3 ML. Note that varying ϵ for Ca_{0.5}TaO₃ in the range 20–30 changes $t_C(\epsilon)$ to 2.5–3.5. Thus, the value of t_C , i.e., ≈ 3 ML of Ca_{0.5}TaO₃, obtained from the present GGA calculations is found to be consistent with the phenomenological model which is based on the modern theory of polarization. In fact, we also note that t_C for the LaAlO₃/SrTiO₃ heterostructures was estimated to be ≈ 4 ML using GGA,²⁷ despite theoretical calculations underestimating the electronic gap for both LaAlO₃ and SrTiO₃.

It is evident from Fig. 4 that as the ML thickness increases, the VBM of the heterointerface TiO₂ layer of the substrate moves toward lower energy and subsequently holes are introduced in its O 2*p* bands. By requirement of charge neutrality, the holes in the interface TiO₂ layer are compensated by electrons in the surface TaO₂ layer, resulting in a *n*-type film-vacuum interface. However, the Ta 5*d* of the overlayers and the Ti 3*d* bands of the substrate do not mix with the O 2*p* bands of the respective layers. That is, the

p-*d* hybridization gap in the layers remain intact, irrespective of the Ca_{0.5}TaO₃ thickness. For instance, in the 3 ML heterostructure, the O 2*p*-Ta 5*d* energy separation in the surface layer is ≈ 2.4 eV, and for subsequent two subsurface TaO₂ layers, it is found to be 1.6 eV. Similarly, the O 2*p*-Ti 3*d* energy separation in the substrate layers also shows variation with the heterointerface TiO₂ layer showing a gap of 1.4 eV. The subsequent TiO₂ layers into the interior of the substrate show a gap of 1.9 eV. It also needs to be mentioned that the CBM of the substrate layers remains more or less pinned at 1.7 eV above E_F .

In the 4 ML Ca_{0.5}TaO₃/SrTiO₃ heterostructure, the layer wise resolved DOS spectra show a finite contribution to the E_F from both the film and the substrate. In order to understand the dominant orbital states responsible for the hole and electron conduction, we show the layer wise decomposed orbital density of states in Fig. 5. It becomes clear from Fig. 5 that the electron gas at the surface TaO₂ layer is predominantly of Ta 5*d* t_{2g} in nature, while the hole gas formed at the heterointerface TiO₂ is of O 2*p* in character. Thus, the Ca_{0.5}TaO₃/SrTiO₃ heterostructure represents itself as a unique single-tier oxide heterostructure system, where both electron and hole gas are realized.

Furthermore, to obtain the contribution of hole carriers in the conduction process, we integrate the layer projected density of states of the substrate with the integration limits set from Fermi energy to the lower conduction band edge. Note that the integration is carried out within the LAPW spheres and therefore does not account the contributions from the interstitial region. For 2 ML, we find ≈ 0.01 holes residing in the TiO₂ heterointerface, which increases to 0.29 holes and 0.32 holes for the 3 ML and 4 ML Ca_{0.5}TaO₃/SrTiO₃ heterostructures, respectively. Also, we find from layer wise analysis (Fig. 5; the sixth and seventh panels from the top) that the hole concentration in the SrTiO₃ substrate decreases exponentially into its interior. For the TiO₂ layer below the heterointerface, the hole concentration decreases by an order of magnitude. Similarly, we also estimated the electron concentration in the conduction process by integrating the layer wise density of states from the bottom of the Ta 5*d* band edge to the Fermi energy. For the 2 ML thickness heterostructure, we found 0.04 electrons in the surface layer, which

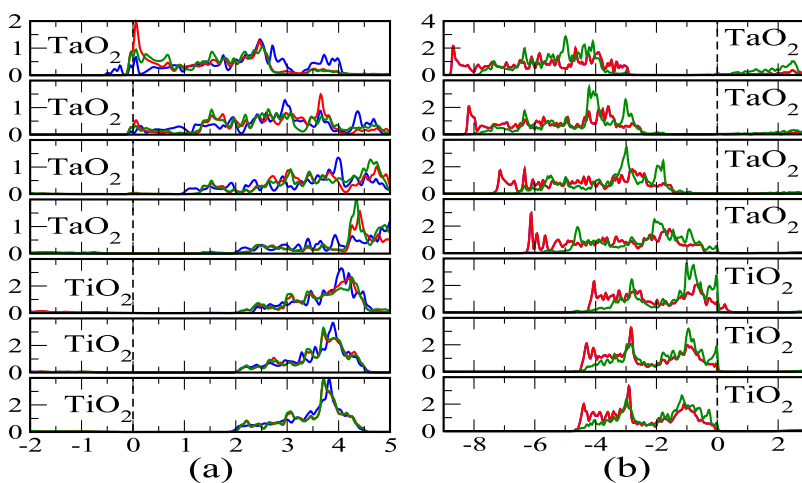


FIG. 5. The layer decomposed (a) Ta 5*d* t_{2g} and (b) O 2*p* resolved partial DOS of the transition metal-oxide layers of the 4 ML Ca_{0.5}TaO₃/SrTiO₃ heterostructure. In (a), the blue, red, and green curves represent the orbital resolved d_{xy} , d_{xz} , and d_{yz} partial density of states, respectively, while in (b) the red and green curves represent the orbital resolved $p_x(p_y)$ and p_z partial DOS, respectively. The top panel represents the surface TaO₂ layer, and the second to fourth panels from the top represent the subsequent TaO₂ layers. The fifth panel from the top represents the TiO₂ heterointerface, whereas the sixth and seventh panels represent the TiO₂ layers of the SrTiO₃ substrate interior. The vertical broken line through energy zero represents the reference Fermi energy.

increased to 0.19 electrons and 0.22 electrons in the 3 ML and 4 ML heterostructures, respectively. However, the surface electron gas was found to decay at a lesser rate into the film interior, in comparison to the hole gas. Our analysis shows that the electron concentration in the subsurface TaO₂ amounts to one-fourth of the concentration determined in the surface TaO₂ layer.

Thus, it becomes evident that in the Ca_{0.5}TaO₃/SrTiO₃ heterostructure, hole conduction occurs at the TiO₂ heterointerface and electron conduction occurs at the surface TaO₂ layers. The partial filling of the Ta 5*d*_{2g} bands thus leads to the formation of mixed valence states associated with the Ta ions, such as Ta⁵⁺, Ta⁴⁺, and/or Ta³⁺ states. Note that charge neutrality conditions applied to bulk Ca_{0.5}TaO₃ render the Ta ions to exist in +5 formal valence state. However, the theoretical observation of charge disproportionation in TaO₂ surface layers should be explored experimentally. To strictly quantify the Ta mixed valence states in the overlayers, one useful analysis may be the core level spectra obtained from the photoemission experiments.

To have an insight of the relative bandwidth associated with the electron and hole bands, as shown in Fig. 6, we show the band structure of the 4 ML Ca_{0.5}TaO₃/SrTiO₃ heterostructure. We find that the Fermi energy crosses the highly dispersive bands of Ta 5*d* character, thereby illustrating a smaller effective mass. On the other hand, the O 2*p* hole states emanating from the TiO₂ heterointerface appear to be lesser dispersive. The states derived from the O 2*p*_{x(y)} bands are spread over the energy range $0.3 \leq E$ (eV) ≤ -0.4 , while the O 2*p*_z bands are very much localized with their energy spread being $0.03 \leq E$ (eV) ≤ -0.03 . The relatively larger bandwidth of the O 2*p*_{x(y)} bands, i.e., ≈ 0.7 eV, in comparison to the out-of-plane O 2*p*_z bands, shows a greater degree of covalent bonding characteristics within the plane, attributing to spatially confined hole gas at the interface.

Finally, in Fig. 7, we show the schematic diagram of band alignment before and after electronic reconstruction in the

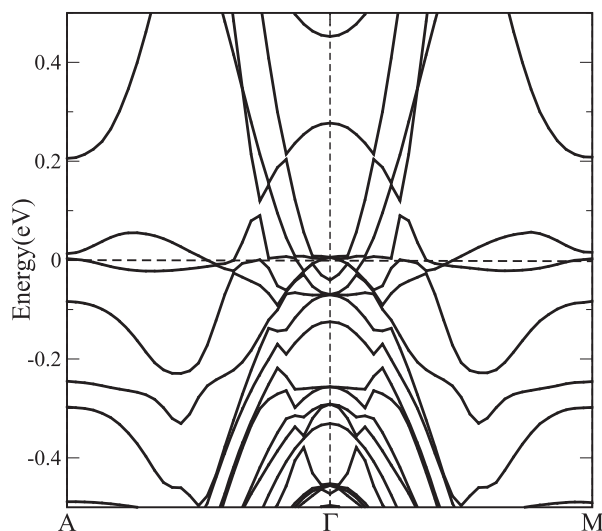


FIG. 6. The band structure of the structurally relaxed 4 ML Ca_{0.5}TaO₃/SrTiO₃ heterostructure, computed using GGA-PBE. The energy zero represents the reference Fermi energy.

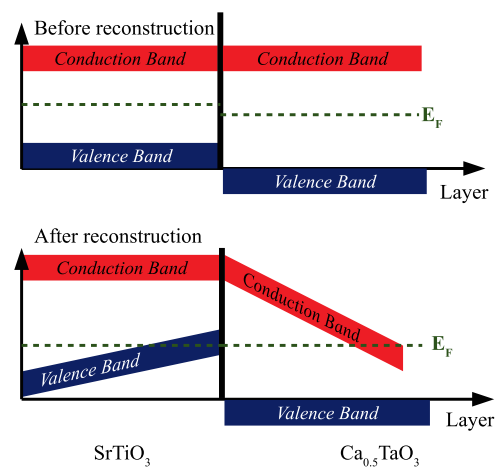


FIG. 7. Schematic plot of the band bending due to the electronic reconstruction in Ca_{0.5}TaO₃/SrTiO₃ with respect to Ca_{0.5}TaO₃ layers.

Ca_{0.5}TaO₃/SrTiO₃ heterostructure. The experimental electronic gap of SrTiO₃ in bulk is 3.3 eV, while that of Ca_{0.5}TaO₃ is 4 eV. As evident from DOS spectra in the Ca_{0.5}TaO₃/SrTiO₃ heterostructure, the conduction band offset is small. The conduction band is mainly composed of the Ta 5*d* and Ti 3*d* states, with the latter being only 0.5 eV above the Ta 5*d* band edge. Thus, the upper edge of these states can be considered as almost aligned. For the electronic reconstruction to occur, a large band bending with the CBM of Ca_{0.5}TaO₃ at the surface aligning with the VBM of SrTiO₃ is required, which is consistent with the observation made in the density functional based calculations presented above. Overall, we find that ML dependent hole and electron conductivity at the TiO₂ heterointerface layer and TaO₂ surface layer in the Ca_{0.5}TaO₃/SrTiO₃ heterostructure is mediated by a rigid band shift of the substrate SrTiO₃ valence and overlayer Ca_{0.5}TaO₃ conduction band, toward the Fermi energy. The calculations, which are based on an abrupt interface/surface, devoid of any oxygen defects, intersite disorder and/or surface adsorbents, relate the underlying conducting mechanism in the Ca_{0.5}TaO₃/SrTiO₃ heterostructure to the polar catastrophe model.

The occurrence of q-2DHG at the interface of insulating oxides heterostructures is rare. In pursuit to look for q-2DHG in single-tier oxide heterostructures, we adhere to the postulates of polar catastrophe theory, i.e., to look for an oxide material which would have a negatively charged layer in contact with the TiO₂ layer of the substrate SrTiO₃ and also that the lattice mismatch be minimal. We find Ca_{0.5}TaO₃ as a good candidate material to exhibit q-2DHG. Modeling the heterostructures by means of supercells, first-principles density functional theory calculations were performed. The electronic structure of the heterostructures shows an evolution of q-2DHG with increasing Ca_{0.5}TaO₃ overlayer thickness on TiO₂ terminated SrTiO₃. The critical thickness of Ca_{0.5}TaO₃ for the existence of q-2DHG was determined to be 3 ML from the GGA-PBE calculations, which is consistent with the empirical model based on the modern theory of polarization. Furthermore, the systematic variations in the interplanar distances between the (Ca_{0.5}O)⁻ and (TaO₂)⁺ charged layers clearly manifest as the response of the built-in electric field, as

predicted by the polar catastrophe theory. The q-2DHG is found to be highly confined to the TiO_2 heterointerface and is derived from the O $2p$ bands. On the other hand, the charge compensated electron carriers are found to reside at the TaO_2 surface layer. The partial filling of the Ta $5d_{2g}$ manifold indicates an electronic reconstruction at the surface, thereby inducing the mixed valence state of the Ta ions. Our argument of charge disproportionation in surface TaO_2 layer in $\text{Ca}_{0.5}\text{TaO}_3/\text{SrTiO}_3$ heterostructures, however, should be explored experimentally. To the best of our knowledge, the $\text{Ca}_{0.5}\text{TaO}_3/\text{SrTiO}_3$ appears as the first single-tier oxide heterostructure in which hole gas exists at its heterointerface. In fact, in heterostructures representing the coupled quantum well system, the interaction between the interface and surface confined charges is expected to drive several novel properties.

The author thank Ajay K. Shukla for discussions and critical reading of the manuscript. This work was supported by the Science and Engineering Research Board (SERB), DST, India, under the project Grant No. EMR/2014/001004.

REFERENCES

- ¹A. Ohtomo and H. Y. Hwang, *Nature* **427**, 423 (2004).
- ²N. Nakagawa, H. Y. Hwang, and D. A. Muller, *Nat. Mater.* **5**, 204 (2006).
- ³N. C. Bristowe, P. Ghosez, P. B. Littlewood, and E. Artacho, *J. Phys.: Condens. Matter* **26**, 143201 (2014).
- ⁴L. Yu and A. Zunger, *Nat. Commun.* **5**, 5118 (2014).
- ⁵J. Mannhart, D. H. A. Blank, H. Y. Hwang, A. J. Millis, and J. M. Triscone, *MRS Bull.* **33**, 1027 (2008).
- ⁶S. A. Pauli and P. R. Willmott, *J. Phys.: Condens. Matter* **20**, 264012 (2008).
- ⁷M. S. Park, S. H. Rhim, and A. J. Freeman, *Phys. Rev. B* **74**, 205416 (2006).
- ⁸R. Pentcheva and W. E. Pickett, *Phys. Rev. B* **74**, 035112 (2006).
- ⁹P. Zubko, S. Gariglio, M. Gabay, P. Ghosez, and J.-M. Triscone, *Annu. Rev. Condens. Matter Phys.* **2**, 141 (2011).
- ¹⁰Y.-Y. Pai, A. Tylan-Tyler, P. Irvin, and J. Levy, *Rep. Prog. Phys.* **81**, 036503 (2018).
- ¹¹Z. Huang, A. Xiao, R. Wang, A. Rusydi, J. Chen, H. Yang, and T. Venkatesan, *Adv. Mater.* **30**(47), 1802439 (2018).
- ¹²M. Huijben, D. Kockmann, J. Huijben, J. E. Kleibecker, A. van Houselt, G. Koster, D. H. A. Blank, H. Hilgenkamp, G. Rijnders, A. Brinkman, and H. J. W. Zandvliet, *Phys. Rev. B* **86**, 035140 (2012).
- ¹³R. Pentcheva, M. Huijben, K. Otte, W. E. Pickett, J. E. Kleibecker, J. Huijben, H. Boschker, D. Kockmann, W. Siemons, G. Koster, H. J. W. Zandvliet, G. Rijnders, D. H. A. Blank, H. Hilgenkamp, and A. Brinkman, *Phys. Rev. Lett.* **104**, 166804 (2010).
- ¹⁴S. Ishibashi and K. Terakura, *J. Phys. Soc. Jpn.* **77**, 104706 (2008).
- ¹⁵H. Lee, N. Campbell, J. Lee, T. J. Asel, T. R. Paudel, H. Zhou, J. W. Lee, B. Noesges, J. Seo, B. Park, L. J. Brillson, S. H. Oh, E. Y. Tsymbal, M. S. Rzchowski, and C. B. Eom, *Nat. Mater.* **17**, 231 (2018).
- ¹⁶S. Gražulis, D. Chateigner, R. T. Downs, A. T. Yokochi, M. Quirós, L. Lut-terotti, E. Manakova, J. Butkus, P. Moeck, and A. Le Bail, *J. Appl. Cryst.* **42**, 726 (2009).
- ¹⁷See <http://www.crystallography.net/cod/> for open-access collection of crystal structures of organic, inorganic, metal-organics compounds and minerals, excluding biopolymers.
- ¹⁸M. Gasperin, *Acta Cryst.* **12**, 422 (1959).
- ¹⁹P. Blaha, K. Schwarz, G. Madsen, D. Kvasicka, and J. Luitz, *Computer Code WIEN2K* (Technical University of Vienna, Vienna, 2001).
- ²⁰J. P. Perdew, K. Burke, and M. Ernzerhof, *Phys. Rev. Lett.* **77**, 3865 (1996).
- ²¹K. Domen, M. Hara, J. N. Kondo, T. Takata, A. Kudo, H. Kobayashi, and Y. Inoue, *Korean J. Chem. Eng.* **18**, 862 (2001).
- ²²U. Schwingenschlögl and C. Schuster, *Europhys. Lett.* **86**, 27005 (2009).
- ²³R. Pentcheva and W. E. Pickett, *J. Phys.: Condens. Matter* **22**, 043001 (2010).
- ²⁴R. Pentcheva, R. Arras, K. Otte, V. Ruiz, and W. E. Pickett, *Philos. Trans. R. Soc., A* **370**, 4904 (2012).
- ²⁵S. A. Pauli, S. J. Leake, B. Delley, M. Björck, C. W. Schneider, C. M. Schlepütz, D. Martocchia, S. Paetel, J. Mannhart, and P. R. Willmott, *Phys. Rev. Lett.* **106**, 036101 (2011).
- ²⁶S. Thiel, G. Hammerl, A. Schmehl, C. W. Schneider, and J. Mannhart, *Science* **313**, 1942 (2006).
- ²⁷A. Rastogi, J. J. Pulikkotil, S. Auluck, Z. Hossain, and R. C. Budhani, *Phys. Rev. B* **86**, 075127 (2012).